2-2014

Structure, Dynamics, and Photophysics in the Copper(I) Iodide–Tetrahydrothiophene System

Kylie M. Henline

Charles Wang

Robert D. Pike
William & Mary, rdpike@wm.edu

John C. Ahern

et al.

Recommended Citation

Henline, Kylie M.; Wang, Charles; Pike, Robert D.; Ahern, John C.; and et al., Structure, Dynamics, and Photophysics in the Copper(I) Iodide–Tetrahydrothiophene System (2014). *Crystal Growth & Design*, 14(3), 1449-1458.
https://doi.org/10.1021/cg500005p

Structure, Dynamics, and Photophysics in the Copper(I) Iodide-Tetrahydrothiophene System.

*Kylie M. Henline, Charles Wang, and Robert D. Pike**

Department of Chemistry, College of William and Mary, Williamsburg, VA 23187-8795.

John C. Ahern, Bryer Sousa, and Howard H. Patterson

Department of Chemistry, University of Maine, Orono, ME 04469-5706.

Andrew T. Kerr and Christopher L. Cahill

Department of Chemistry, The George Washington University, Washington, DC 20052.

Email address: rdpike@wm.edu

RECEIVED DATE (to be automatically inserted after your manuscript is accepted if required according to the journal that you are submitting your paper to)

*Corresponding author. (RDP) Tel: 757-2212555; fax: 757-2212715.

ABSTRACT Combination of CuI and tetrahydrothiophene (THT) in MeCN or neat THT produces various phases depending upon experimental conditions. Green luminescent product $(CuI)_4(THT)_2$ (**1**) consists of Cu_4I_4 cubane units knit into a 3-D network by μ_2-THT ligands. Yellow luminescent $(CuI)_{10}(THT)_7(MeCN)$ (**2**) contains {[Cu_4I_4(THT)](μ_2-THT)$_2$(Cu_2I_2)(μ_2-THT)$_2$[Cu_4I_4(NCMe)]} "rungs" linked into 1-D ladders by pairs of μ_2-THT ligands. Two molecular $(CuI)_4(THT)_4$ phases were found:

orange luminescent **3a** and dull yellow luminescent **3b**. Triclinic **3b** is the more stable phase at 25 °C, but undergoes endothermic transformation to monoclinic **3a** at 38 °C. **3a** transforms to a triclinic phase (**3a'**) that retains orange emission at −60 °C. Non-emissive $(CuI)_3(THT)_3$•MeCN (**4**) is a 2-D sheet structure in which $Cu_3(THT)_3$ rings are linked in trigonal directions by rhomboid Cu_2I_2 dimer units. The previously reported $(CuI)_2(THT)_4$ (**5**) is a molecular dimer. Temperature and mixing ratio domains for the formation of the CuI-THT phases from MeCN are presented. Luminescence in **1**, **2**, **3a**, and **3b** is rationalized based on varying degrees of halide-to-metal charge transfer (XMCT) and metal-centered (MC) behavior. Low temperature spectra reveal reversible changes, including modest red shifts for **1** and **2**, and splitting into two excitation/emission band pairs for **3a** and **3b**.

Introduction

The complexes of copper(I) iodide with nitrogen, phosphorus, and sulfur ligands (L) are of interest both structurally and photophysically. Building upon our own work[1] and that of others[2] involving discrete CuI-L complexes, we have shown that photoluminescent CuI-L adducts form spontaneously when films of CuI are exposed to vapor samples of volatile amines or sulfides.[3] During the course of this work, we noted remarkable behavior of tetrahydrothiophene (THT) with CuI surfaces, yielding a mixture of green and orange emission under 365 nm irradiation at room temperature, and a strong yellow-green peak at 77 K. These results were highly suggestive of the existence of multiple CuI-THT phases. While multiple stoichiometries are not particularly unusual in CuI-L complexes, it appeared that this system was especially complex. The results of the current study confirm this suspicion. In addition to a previously identified phase,[4] we herein report five new phases that result when CuI and THT are combined in acetonitrile (MeCN). Four of these compounds show luminescence behavior.

The structural chemistry of CuI-sulfide complexes encompasses three major classes, as shown in Scheme 1. A molecular cubane tetramer Cu_4I_4 with monodentate sulfide ligands has been reported,[5] as have numerous molecular Cu_2I_2 dimers[4,6] and a single CuI stair step polymer[7] containing chelating disulfide ligands. Far more common are structures in which bridging disulfide ligands link the rhomboid

dimers, cubane tetramers, or stair step chains into network arrangements.[8,9] Much rarer is the occurrence of CuI cubane tetramers or rhomboid dimers linked into networks by monosulfide ligands in which a single sulfur atom acts as the bridge.[10,11] This phenomenon has only been observed to date for dimethyl sulfide and diethyl sulfide.

Scheme 1

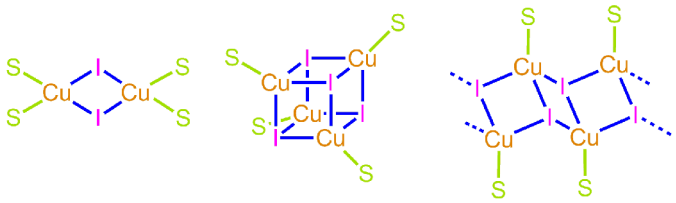

The photophysics of the CuI-L system have been explored computationally by Ford[12] and other researchers.[1,11b,13] The cubane cluster acts as a rather intense luminophore. Most $(CuI)_4L_4$ compounds absorb exclusively in the UV and therefore appear white under visible light. They usually emit in the visible, giving a variety of colored responses under black light. Thermochromism is quite common. Two emission bands are often seen for the $(CuI)_4L_4$ cubanes. The ubiquitous low energy (LE) emission usually occurs in the green-red region. It is attributed to a triplet cluster-centered (^{3}CC) transition, which combines halide-to-metal charge transfer (XMCT) and metal-centered (MC) behavior. Owing to its sensitivity with respect to distortions within the Cu_4I_4 cluster, the ^{3}CC band is subject to significant thermochromic and rigidochromic effects. A second, high energy (HE) emission band in the blue region is typically observed when ligands having π^* orbitals are used. This band is the result of a triplet halide-to-ligand charge transfer (^{3}XLCT). Transitions in CuI dimers[1] and hexamers[9a] have been less extensively studied. However, ^{3}CC and ^{3}XLCT transitions appear to be important in these species as well.

Experimental

Materials and Methods. All reagents were purchased from Aldrich, Acros, or Strem Chemicals and were used as received. Experimental temperatures in the product formation studies were maintained

using either a thermostated refrigerated recirculating bath or thermostated heated oil bath. Analysis for C and H were carried out by Atlantic Microlabs, Norcross, GA. Thermogravimetric analyses (TGA) were conducted using a TA Instruments Q500 in the dynamic (variable temp.) mode with a maximum heating rate of 50 °C/min to 800 °C under 60 mL/min N_2 flow. Differential scanning calorimetry (DSC) was conducted using a TA Instruments Q20 in the ramp mode with a scanning rate of 3 °C/min from 0 to 50 °C.

Steady-state photoluminescence spectra were recorded with a QuantaMaster-1046 photoluminescence spectrophotometer from Photon Technology International. The instrument is equipped with two excitation monochromators and a single emission monochromator with a 75 W xenon lamp. Low temperature steady-state photoluminescence measurements were achieved by using a Janis St-100 optical cryostat equipped with a Honeywell temperature controller. Liquid nitrogen was used as coolant. Steady-state photoluminescence spectra were collected for compounds **1**, **2**, **3a**, and **3b**. Spectra were collected as sequential emission scans to form a 3-D matrix with excitation as the *x* axis, emission on the *y* axis, and intensity on the *z* axis. The wavelength of the exciting light was run from high to low wavelength at increments of 3 nm between 500 and 200 nm to avoid photobleaching, oxidation or other forms of degradation.

For lifetime measurements for **1**, **2**, **3a**, and **3b** at 293 K and 77 K, excitation was provided by an Opolette™ (HE) 355 II UV tunable laser operating at 335 nm. The 335 nm excitation was chosen since all samples could be excited at this wavelength. The laser has a Nd:YAG flashlamp pumped with a pulse repetition rate of 20 Hz and an average output power 0.3 mW. The detection system is composed of a monochromator and photomultiplier from a JobinYvon Ramanor 2000M Raman spectrometer. Data were collected by a Le Croy 9310C dual 400 MHz oscilloscope collecting data every 10 ns for 50 μs per sweep averaging 1000 sweeps per sample. Each sample was run 3 times through this 1000 sweep cycle and the results were averaged. The decay curves from these measurements were fitted using an exponential decay fitting method in Origin Pro 8. The lifetimes were observed at the ideal emission

wavelengths for compounds **1**, **2**, **3a**, and **3b** as determined by luminescence spectroscopy.

Syntheses

$(CuI)_4(THT)_2$, **1.** 2.0 mL of 150 mM CuI in MeCN (0.30 mmol) and 2.0 mL of 250 mM THT in MeCN (0.50 mmol) were combined in a capped vial at 40 °C with stirring. A white precipitate with green luminescence formed immediately. The powder was collected by decanting, washed using ethyl ether, and vacuum dried (0.029 g, 0.031 mmol, 41%). Anal. Calcd. for $C_8H_{16}Cu_4I_4S_2$: C, 10.24; H, 1.72. Found: C, 10.34; H, 1.66. TGA Calcd. for CuI: 81.2. Found: 81.6 (105−125 °C). Crystals of **1** were produced by layering 1.0 mL of 150 mM THT in MeCN (0.15 mmol) over 0.40 mL of 150 mM CuI in MeCN (0.060 mmol) in a capped vial at 40 °C and allowing diffusional mixing at 40 °C.

$(CuI)_{10}(THT)_7(MeCN)$, **2.** 2.8 mL of 150 mM CuI in MeCN (0.42 mmol) and 2.0 mL of 150 mM THT in MeCN (0.30 mmol) were combined in a capped vial at −10 °C with stirring. A white precipitate with yellow luminescence formed immediately. The powder was collected by decanting and immediately placing under vacuum for 2 h (0.065 g, 0.025 mmol, 60%). Anal. Calcd. for $C_{30}H_{59}Cu_{10}NI_{10}S_7$: C, 14.06; H, 2.32. Found: C, 14.17; H, 2.23. TGA Calcd. for CuI: 74.3. Found: 74.5 (80−125 °C). Crystals of **2** were produced by layering 2.0 mL of 150 mM CuI in MeCN with 2.0 mL of 250 mM THT in MeCN and allowing diffusional mixing at room temp.

$(CuI)_4(THT)_4$ (orange emission), **3a.** 2.0 mL of 150 mM CuI in MeCN (0.30 mmol) and 2.0 mL of 400 mM THT in MeCN (0.80 mmol) were combined in a capped vial at room temp. A white precipitate with orange luminescence formed immediately upon stirring. The powder was collected by decanting and immediately placing under vacuum for 2 h (0.035 g, 0.031 mmol, 42%). Anal. Calcd. for $C_{16}H_{32}Cu_4I_4S_4$: C, 17.25; H, 2.87. Found: C, 17.12; H, 2.88. TGA Calcd. for $(CuI)_4(THT)_2$: 84.2. Found: 85.6 (90−100 °C). Calcd. for CuI: 68.4. Found: 70.6 (100−125 °C). Crystals of **3a** were produced by layering 2.0 mL of 150 mM CuI in MeCN with 2.0 mL of 250 mM THT in MeCN and allowing diffusional mixing at room temp.

$(CuI)_4(THT)_4$ (dull yellow emission), **3b.** 1.5 mL of 150 mM CuI in MeCN (0.225 mmol) and 3.0

mL of 150 mM THT in MeCN (0.45 mmol) were combined in a capped vial at 0 °C. A white precipitate with dull yellow luminescence formed immediately upon stirring. The powder was collected by decanting and immediately placing on vacuum for 2 h (0.033 g, 0.030 mmol, 53%). Anal. Calcd. for $C_{16}H_{32}Cu_4I_4S_4$: C, 17.25; H, 2.87. Found: C, 17.03; H, 2.79. TGA Calcd. for $(CuI)_4(THT)_2$: 84.2. Found: 84.5 (60−75 °C). Calcd. for CuI: 68.4. Found: 69.1 (75−115 °C). Crystals of **3b** were produced by layering 1.0 mL of 100 mM CuI in MeCN with 0.35 mL of neat THT and allowing diffusional mixing at 5 °C.

$(CuI)_3(THT)_3$•MeCN, **4.** 0.80 mL of 150 mM CuI in MeCN (0.12 mmol) and 2.0 mL of 150 mM THT in MeCN (0.30 mmol) were combined in a capped vial at −5 °C with stirring. A white precipitate with no luminescence formed immediately (0.012 g, 0.014 mmol, 34%). All attempts to isolate this product with drying caused traces of orange luminescence (indicative of **3a**) to develop immediately, rendering elemental analysis impossible. TGA Calcd. for $(CuI)_4(THT)_4$: 95.3. Found: 95.2 (40−55 °C). Calcd. for $(CuI)_4(THT)_2$: 80.2. Found: 79.7 (80−105 °C). Calcd. For CuI: 65.2. Found: 64.6 (125−140 °C). Crystals of **4** were produced by layering 2.0 mL of 150 mM CuI in MeCN with 5.0 mL of 150 mM THT in MeCN and allowing diffusional mixing at −8 °C.

$(CuI)_2(THT)_4$, **5.** CuI (0.50 g, 2.6 mmol) was dissolved in 0.46 mL (5.3 mmol) neat THT in a capped vial at room temp. A white precipitate with no luminescence formed upon sonication. The powder was collected on a frit under vacuum (0.84 g, 1.1 mmol, 88%). All attempts to isolate this product with drying caused traces of orange luminescence (indicative of **3a**) to develop rapidly, rendering elemental analysis impossible. TGA Calcd. for $(CuI)_4(THT)_4$: 76.0. Found: 77.1 (45−75 °C). Calcd. For CuI: 51.9. Found: 52.7 (95−145 °C). Crystals of **5** were synthesized by producing a saturated solution of CuI in neat THT and storing at −8 °C.

X-ray Analysis: Crystals were mounted on glass fibers and analyzed at 100 K, except for **3a** which was run at 250 K. Crystals of **4** and **5** were highly sensitive to solvent loss and were coated in Paratone

N oil and flash-cooled to 100 K. All measurements were made using graphite-monochromated Cu Kα radiation on a Bruker-AXS three-circle diffractometer, equipped with a SMART Apex II CCD detector.[14] Initial space group determination was based on a matrix consisting of 120 frames. The data were reduced using SAINT+,[15] and empirical absorption correction applied using SADABS.[16]

Structures were solved using SIR-92[17] or SHELX.[18] Least-squares refinement was carried out for all structures on F^2 using SHELX-13 and ShelXle.[19] The non-hydrogen atoms were refined anisotropically. In all cases, hydrogen atoms were located the Fourier difference map and then placed in theoretical positions. Details of the X-ray experiments and crystal data are summarized in Table 1. Selected bond lengths and bond angles are given in Table 2. Crystallographic data for new structures reported herein were deposited with the Cambridge Crystallographic Data Centre and allocated the deposition numbers CCDC 977480-977484. These data can be obtained free of charge from the Cambridge Crystallographic Data Centre via www.ccdc.cam.ac.uk/data_request/cif.

Powder X-ray diffraction (PXRD) data for **1**, **2**, **3a**, and **3b** were collected using Rigaku Miniflex diffractometer with Cu Kα radiation. Scans were carried out from 3 to 60° 2 theta at 2 deg./min. For compound **3b** a 10 h scan was necessary due to weak response. In this case, the compound was mulled with Paratone N oil to prevent its conversion to **3a**. The data were processed using the MDI-Jade 6.1 software package.[20] Powder X-ray diffraction (PXRD) data for **4** and **5** were collected using Bruker instrument described above as mulls using Paratone N oil. Three 180 s frames were collected, covering 5–60º 2θ. Frames were merged using the SMART Apex II software[14] and were further processed using DIFFRAC-Plus and EVA software.[21] All calculated powder patterns from single crystal structural data were produced using Mercury software.[22]

Results and Discussion

CuI-THT Phases

Following our previous observation of multiple luminescence emission colors in CuI films that had

been exposed to THT vapor (see Introduction),[3] an initial crystallization experiment with CuI and THT in MeCN was carried out. In this case 35 μL THT were added to one mL of 40 mM CuI solution in MeCN, following which the mixture allowed to stand at ambient temperature. Visualization of the resulting colorless crystals using 365 nm black light revealed four distinct species: (1) octahedra having green luminescence, (2) prisms having yellow luminescence, (3) prisms having orange luminescence, and (4) prisms having dull yellow luminescence. These phases later proved to be **1**, **2**, **3a**, and **3b**, respectively. The readily observed formation of at least four distinct phases led us to study the CuI-THT system in MeCN carefully. Pre-temperature-equilibrated MeCN solutions of CuI (150 mM) and THT (150 mM) were combined in capped vials and stirred at controlled temperature. In all cases white precipitates formed over the course of several minutes to several hours, excepting relatively CuI-rich mixtures at relatively high temperatures which failed to afford solid. The identities of the solid products were assigned initially via observation of luminescence emission color, and then further confirmed through a combination powder X-ray diffraction (PXRD) and thermogravimetric analysis (TGA), as described below. The results of this phase domain study are shown in Figure 1.

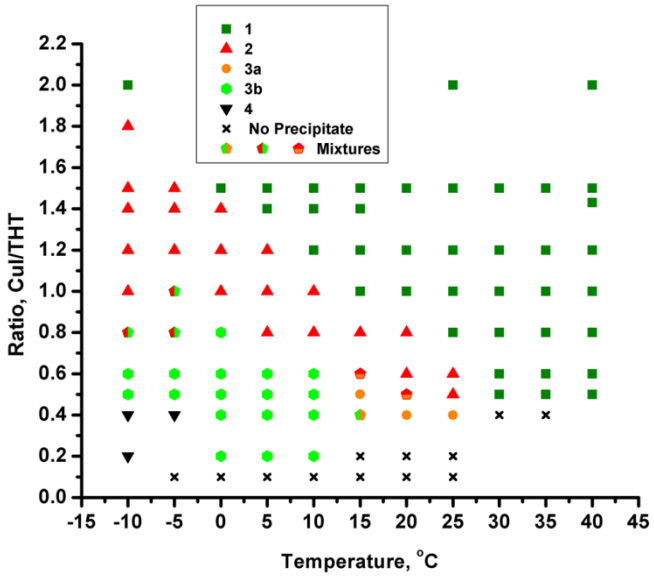

Fig. 1. Precipitate domains for CuI/THT mixtures in MeCN at various mixing ratios and temperatures.

Five phases were identified during the above study. At relatively high temperatures and high CuI contents, a green-emitting phase having the stoichiometry $(CuI)_4(THT)_2$ (**1**) precipitated. At somewhat lower temperatures and CuI contents, a dull yellow-emissive phase was formed. This proved to have the unusual formulation $(CuI)_{10}(THT)_7(MeCN)$ (**2**). In a very limited domain near room temperature, but with very low CuI concentration, an orange-emitting precipitate was formed. This material proved to be a cubane compound $(CuI)_4(THT)_4$ (**3a**). If, instead of lowering CuI amount from the **2** domain, the temperature was lowered, a different $(CuI)_4(THT)_4$ cubane, having yellow emission (**3b**) was produced. Finally, at temperatures <0 °C and very low CuI amounts, a non-emissive phase having the formula $(CuI)_3(THT)_3$•MeCN (**4**) was formed. Not found in any of the precipitation products from MeCN was the known phase $(CuI)_2(THT)_4$ (**5**), for which the question of photoluminescence was not addressed in the literature report (it proved to be non-emissive).[4]

Samples of the CuI-THT phases **1**, **2**, **3a**, **3b**, and **4** were synthesized according to optimized conditions as suggested by the results in Figure 1. Non-emissive compound **5** was prepared following a modification of the literature procedure in which CuI (rather than Cu/KI) was dissolved in neat THT.[4] Blacklight photos under 365 nm excitation of the four emissive phases **1**, **2**, **3a**, and **3b** are shown in Figure 2. The compounds **1**−**5** were studied using a variety of techniques including TGA (Figure 3), single crystal X-ray diffraction, PXRD (Figures S12−S17, Supporting Information), and elemental analysis. However, compounds **4** and **5** proved to be highly susceptible to loss of MeCN and THT respectively, making elemental analysis impossible in these cases. These non-emissive compounds quickly developed patches of orange luminescence upon drying, indicating partial conversion to **3a**. For all six TGA traces, the sample mass remaining after the temperature had reached 150 °C corresponded very closely to the % CuI in the initial complex. Initial mass loss temperatures were consistent with the relative stabilities noted for the complexes during routine handling. Thus, the particularly stable **1** did not lose mass until 105 °C. Compounds **2** and **3a** were somewhat less stable, showing mass losses commencing below 100 °C. Compound **3b** proved less stable to heating than **3a** by differential scanning

calorimetry (DSC, see below). Accordingly, **3b** underwent mass loss beginning at 60 °C, 30 °C below the analogous point for **3a**. Mass losses for **4** and **5** began at very modest temperatures, with a clear MeCN loss step evident for **4**.

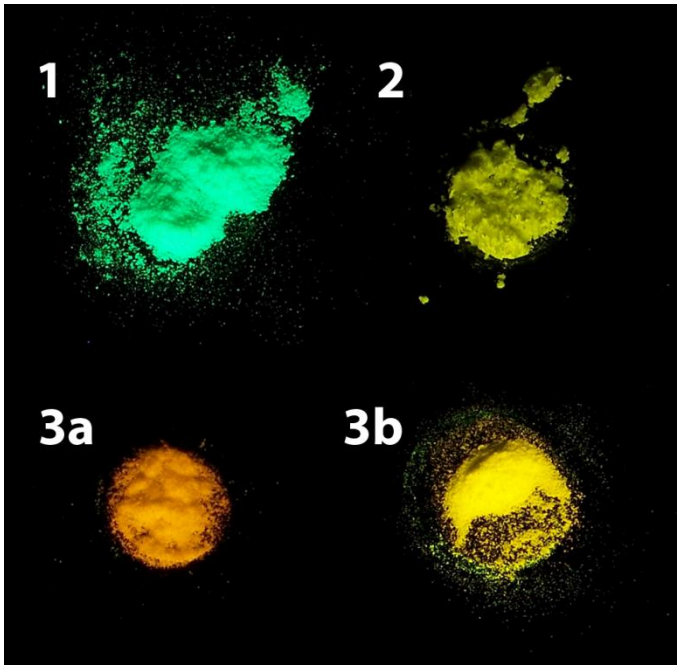

Fig. 2. Photographs of emissive phase samples under 365 nm excitation.

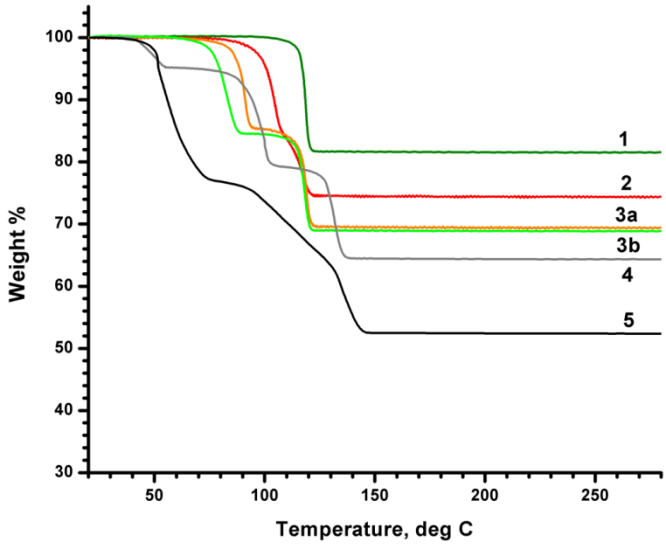

Fig. 3. TGA traces for CuI-THT phases.

X-ray Structures

Crystals were grown for the five new compounds in the current study, and the X-ray structures were solved. Refinement details for all structures are summarized in Table 1 and selected bond lengths and angles are given in Table 2. All new structures were tested for porosity using PLATON SQUEEZE, which identifies voids having spherical radii of ≥1.2 Å.[23] No significant voids were found in any case.

Complex **1** crystallizes in non-centrosymmetric space group $P2_12_12_1$ with a degree of racemic twinning present (Flack parameter = 0.138(12)). Its structure is shown in Figures 4, S1, and S2. The repeat unit consists of a Cu_4I_4 cubane unit and two THT ligands. These ligands bridge cubane units through single sulfur atoms, forming a 3-D network. This results in a degree of crowding which is apparent in some unusual compressed and open I−Cu−S bond angles, especially around Cu4 (range = 93.64(12)−117.00(13)°). Single-sulfur bridging of CuI clusters is very rare, having been previously reported only in $[(CuI)_4(Me_2S)_3]$ and $[(CuI)_4(Et_2S)_3]$.[10,11] Neither of these previous structures contains true "closed" cubanes. In $[(CuI)_4(Me_2S)_3]$ the cubanes are opened, such that only three Cu atoms show the usual I_3S coordination sphere, while the fourth Cu atom has an I_2S_2 environment; all THT ligands are μ_2-bridging, affording a 3-D network. In $[(CuI)_4(Et_2S)_3]$, 1-D chains of $(THT\text{-}Cu)_2(\mu_2\text{-}I_2)$ dimers result from μ_2-bridging by a third THT ligand. In contrast, the closed cubane units in **1** are linked to form puckered $(Cu_4I_4)_6(\mu_2\text{-}THT)_6$ rings. These rings are found in each of three orthogonal directions, coming together at cubane nodes. In this regard the current structure more closely resembles other cubane networks that are linked by disulfide ligands, such as $EtS(CH_2)_4SEt$.[8c] The latter networks tend to contain more open space due to their longer bridges. The cuprophilic Cu···Cu distances (2.636(3)−2.759(3) Å) are slightly shorter than that van der Waals radius sum of 2.8 Å, as is typical for Cu_4I_4 cubanes. Bond lengths and angles in **1** are otherwise relatively unremarkable.

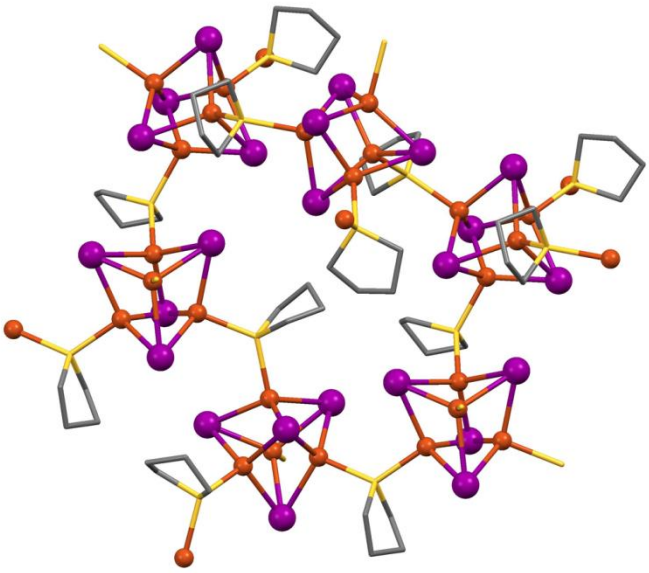

Fig. 4. X-ray structure of **1**. Key to Figs. 4–8: Copper and iodine atoms shown as spheres. THT ligands are shown as wireframe. Color scheme for all X-ray figures: orange = Cu, purple = I, yellow = S, grey = C, blue = N. Hydrogen atoms omitted.

The X-ray structure of **2** (Figures 5 and S3−S5) is complex and unprecedented, the crystallographically independent unit containing eight unique Cu atoms, seven unique I atoms, and six unique THT ligands. It crystallizes in the monoclinic $P2_1/m$ space group, but with significant disorder in the three THT ligands that lie on the crystallographic mirror plane. In addition, the Cu atom bearing the MeCN ligand is disordered over two sites (Cu8 and Cu9). Two independent cubane units are present. Atoms Cu3, Cu4, Cu4' (prime indicates a mirror symmetry position), Cu5 and I2, I3, I4, I4' form an open cubane, similar to that described above for $[(CuI)_4(Me_2S)_3]$. Thus, Cu3, Cu4, and Cu4' have I_3S coordination, while Cu5 has I_2S_2. One of these THT ligands (containing S4 atom) on Cu5 is monodentate. Cu3 and Cu5 are bridged by μ_2-THT ligands (S1 and S2 atoms) to a central rhomboid dimer Cu_2I_2 (Cu1, Cu2, I1 and I1'). The other side of this dimer is bridged through two more μ_2-THT ligands (S5 and S6 atoms) to another cubane (Cu6, Cu7, Cu7', Cu8/9, I5, I6, I7, and I7'). This cubane is also open when reckoned using Cu8 (90% occupancy, see Figure 5), but "closed" when containing Cu9

(10% occupancy, see Figure S3). The sole MeCN ligand on Cu8 is analogous to the S3 THT insofar as it acts a monodentate capping ligand. The (Cu_4I_4)-$(\mu_2$-THT$)_2$-(Cu_2I_2)-$(\mu_2$-THT$)_2$-(Cu_4I_4) structure thus described forms a long 1-D chain (I3···I6 = 18.7 Å). These chains are knit together like rungs on a ladder by bridging μ_2-THT (S3 atom) ligands which link Cu4 and Cu7. The ladders are not further crosslinked into 2-D sheets, but the direction of the rungs (Cu4−Cu7 *vs.* Cu7−Cu4) alternates along each ladder. The cuprophilic Cu···Cu distances from the cubane Cu's to the "swung out" Cu (Cu3···Cu5 = 2.691(4), Cu6···Cu8 = 2.601(4) Å) do not significantly differ from those within the cubanes (Cu3···Cu4 = 2.700(3), Cu6···Cu7 = 2.680(3) Å). The Cu···Cu spacing in the dimer (Cu1···Cu2) is somewhat longer at 2.754(3) Å, but all Cu···Cu in **2** are less than the van der Waals sum value. The Cu−I−Cu bond angles in both dimer and cubane clusters tend to be in the range of 58−63°; however, in the present case, there are two outlying values: Cu8−I7−Cu7' = 192.70(8) and Cu5−I4−Cu4' = 97.58(7). These are the result of the opening of the cubanes.

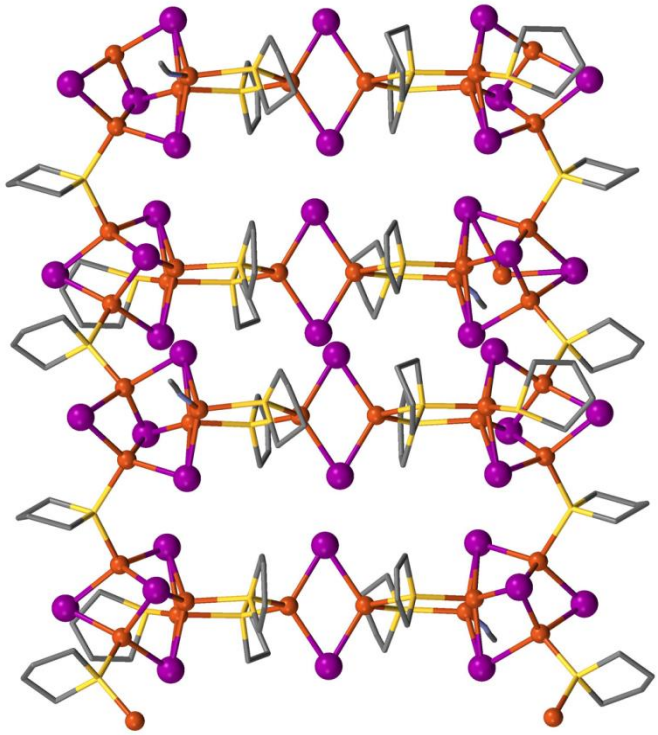

Fig. 5. X-ray structure of **2**. Disordered Cu9 (10% occupancy) and hydrogen atoms omitted.

Compounds **3a** and **3b** are polymorphs, each having the simple cubane formula $(CuI)_4(THT)_4$ (Figures 6 and S6−S8). Formation of a pair of cubane polymorphs has previously been described for $(CuI)_4(PPh_3)_4$, which (like **3a** and **3b**) also showed luminescence emission that differed between the two polymorphs.[24] The X-ray structure of **3a** was analyzed at 250 K because of a destructive phase change that occurred at 213 K producing a triclinic cell (see below). The monoclinic structure for **3a** ($P2_1/n$) shows two crystallographically independent cubane units in the unit cell. One of these contains a disordered THT in which two ligand positions are bonded to Cu8. Polymorph **3b** crystallizes in the triclinic $P\bar{1}$ space group with a single cubane molecule showing no disorder. Bond lengths and angles reveal no meaningful differences amongst the three cubanes in **3a** and **3b**: For example, Cu−I distances in **3a** are 2.651(2)−2.710(2) and 2.647(2)−2.709(3) Å, and in **3b** are 2.650(3)−2.728(3) Å; and Cu···Cu distances in **3a** are 2.673(2)−2.761(2) and 2.669(2)−2.837(3) Å, and in **3b** are 2.639(3)−2.768(3) Å.

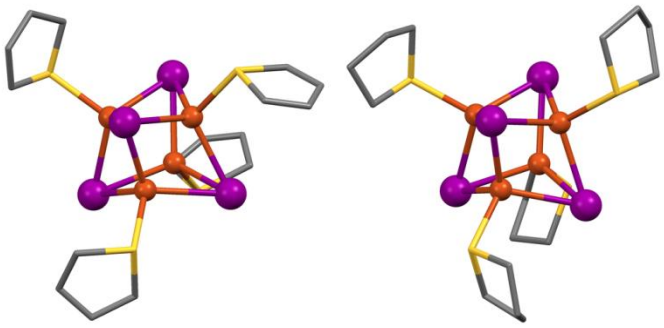

Fig. 6. X-ray structures of **3a** (left) and **3b** (one molecule only shown, right). Hydrogen atoms omitted.

As is the case with **1** and **2**, compound **4**, $(CuI)_3(THT)_3$•MeCN, shows bridging THT behavior leading to network formation (Figures 7 and S9−S11). It crystallizes in the monoclinic $C2/c$ space group and contains a non-coordinated MeCN molecule. The crystallographically independent unit consists of three each Cu, I, and THT, and a single disordered MeCN. Dimeric Cu_2I_2 units are linked via μ_2-THT to form six-membered Cu_3S_3 rings. These rings are further tiled into $(Cu_2I_2)_6(THT)_6$ macrocycles which form nearly flat 2-D sheets. The THT rings point toward the centers of these larger rings. The MeCN

molecules are trapped between the 2-D sheets, being aligned with the center of the large rings. The separation between the 2-D sheets is quite small with an interplanar I···I distance of about 4.3 Å. Once again, fairly short Cu···Cu interactions (2.9653(14), 2.9722(9) Å) are present in the Cu_2I_2 units; however, in this compound they are longer than the van der Waals sum. This effect is further reflected in the relatively open Cu−I−Cu bond angles of 69.06(3)−69.43(2)°.

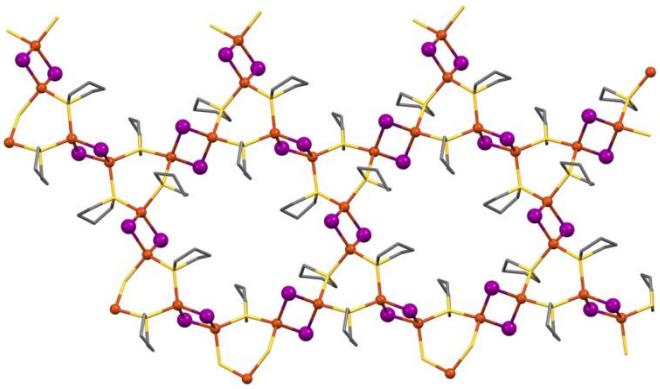

Fig. 7. X-ray structure of **4**. MeCN molecule and hydrogen atoms omitted.

The final CuI-THT compound identified herein, **5**, has previously been characterized at 200 K as the simple dimer $(CuI)_2(THT)_4$ (Figure 8).[4] Cu−I distances of 2.637(1) and 2.639(1) Å, and Cu−S distances of 2.331(3) and 2.318(2) Å are well within the ranges seen for compounds **1**−**4**. A single independent Cu···Cu cuprophilic interaction of 2.675(2) Å was noted.

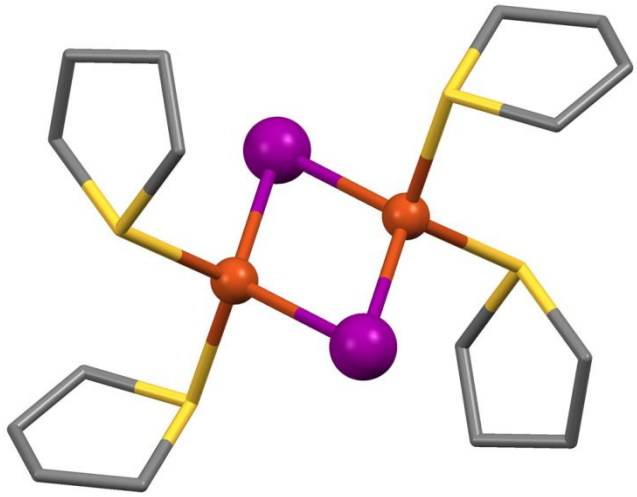

Fig. 8. X-ray structure of **5**.[4] Hydrogen atoms omitted.

Freshly prepared bulk samples of all complexes were examined by PXRD and their patterns compared to those calculated from the X-ray crystal structures (Figures S12−S17). Compounds **1**, **2**, and **3a** yielded excellent matches between experimental and calculated data. Oddly, compound **3b** showed very weak response by PXRD. A ten-hour scan carried out under oil showed only weak response from the compound, which must be presumed to have lost its crystallinity. This lengthy scan brought out minor impurity peaks. As noted above, compounds **4** and **5** were very susceptible to loss of MeCN and THT, respectively. In these cases it was necessary to flash freeze an oil suspension of the compound in order to collect the PXRD data. Although these patterns also showed evidence of minor impurities, presumably due to loss of volatiles, they matched the calculated patterns of **4** and **5**, respectively.

Phase Conversion Studies

The existence of multiple phases containing only CuI and THT presented the opportunity to study the interrelationship between them. Differential scanning calorimetry (DSC) was used to examine the conversion between polymorphs **3a** (orange emission) and **3b** (dull yellow emission) at modest temperatures. As can be seen in Figure 9, an endothermic transition was apparent for **3b** at 38 °C. This presumably corresponded to the conversion **3b** → **3a**. In order to confirm this hypothesis, separate dry samples of **3a** and **3b** were heated to 35 and 45 °C in an oil bath while observing their luminescence emission color. At 45 °C the dull yellow emissive **3b** sample was seen to convert to orange emissive **3a** over the course of about an hour, while the **3a** sample remained unchanged. At 35 °C the opposite transformation behavior was observed (**3a** → **3b**, **3a** remaining unchanged), this time taking overnight due to significant activation energy in the solid state. In the precipitation study from MeCN solution described above (see Figure 1), **3a** also proved to be the $(CuI)_4(THT)_4$ polymorph formed at higher temperatures. The density of **3b** (2.588 g/cm^3) exceeds that of **3a** (2.461 g/cm^3). Thus, according to

Kitaigorodskii's rule,[25] it is expected that **3b** is the more stable form at room temperature. This appears to be the case based on the results from DSC and controlled temperature solid state reactions. However, **3a** seems to be the kinetically favored product based on the grinding studies described below.

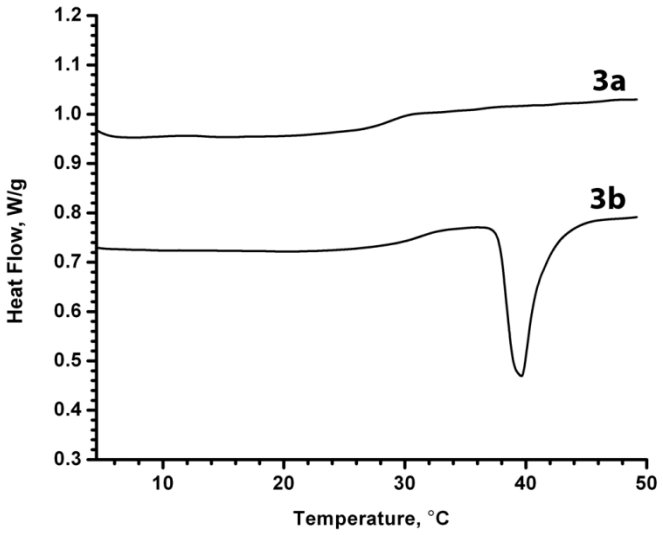

Fig. 9. DSC traces for **3a** and **3b**.

There appears to be yet another phase transition accessible to this system. When crystals of **3a** were cooled on the diffractometer, a phase change was seen in the diffraction pattern at 213 K (−60 °C). Cooling of the crystals below 213 K invariably caused them to crack. As a result, their diffraction was rendered of lower quality, even after the sample was re-warmed back above 213 K. Of importance was the fact that the orange emission persisted when the sample was cooled through the phase change down to temperatures as low as 100 K. Therefore, it was apparent that this phase change did not represent **3a** conversion to **3b**. In fact, compound **3b** itself showed no evidence of any phase change when cooled from ambient temperature to 100 K for data collection. Although the diffraction data of the new low-temperature phase (**3a'**) were not of sufficient quality to allow for structure determination, the unit cell was reliably indexed. Comparison of the unit cell parameters for **3a**, **3a'**, and **3b** is offered in Table 3. Conversion of **3a** to **3a'** appeared to alter the cell parameters only slightly, the major difference being the loss of right angles, producing a triclinic cell. The very modest nature of the phase change is

consistent with a relatively low activation barrier, and therefore kinetically facile phase change observed. Since the cell volume is unchanged, the number of unique cubane molecules present must increase from two in the **3a** unit cell to four in **3a'**, assuming that centrosymmetry is preserved. In contrast to the large unit cell for **3a** and **3a'** in which the number of molecules (Z) is eight, **3b** forms a simpler cell with a single independent cubane and a Z value of two.

Grinding studies were carried out on **1**, **2**, **3a**, and **3b** to examine the mechanochemical conversions of the phases. The product phases noted in Table 4 were initially identified through observation of luminescence emission, and then confirmed via PXRD. Dry grinding of samples in the absence of added THT produced the following results: **1** remained unchanged, **2** → **1**, **3a** → **3a**/**3b** mixture, and **3b** → **1**. Thus, in the absence of added THT, it appears that the more THT-rich phases ultimately convert to the most THT-poor compound **1**. In the case of **3a** added mechanical energy managed to produce some conversion to the thermodynamic product (at ambient temp.), i.e. **3b**. Grinding results were quite different when THT was added to the sample. With a sufficient excess of THT present, all four other compounds converted to the non-emissive **5**. When only a drop of THT was added, grinding of **1**, **2**, or **3b** produced **3a**, which appears to be the kinetically favored of the cubane phases. Overall, it appears that **1** is preferred under moderately THT-deficient conditions, **3a** is produced under moderately THT-rich circumstances, and **5** is preferred in the presence of large THT excesses. These observations are consistent with the crystallization of **5** from neat THT, and also with its facile loss of THT from **5** when left in air to produce **3a**. These results are summarized in Scheme 2. Behavior under vacuum was also studied. Compounds **1** and **2** are not affected by overnight vacuum treatment at 50 mTorr. However, **3a** and **3b** both convert to **1** under these conditions.

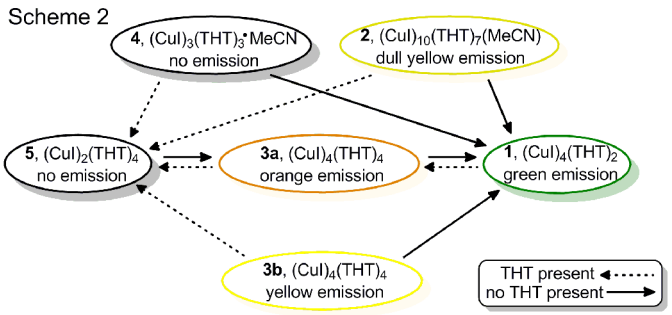

Luminescence Spectroscopy

Four of the six compounds considered herein are strongly photoluminescent, each showing a distinct visible emission color upon irradiation with UV light. Of particular interest was the fact that two of these materials were actually polymorphs of the same compound, $(CuI)_4(THT)_4$, which appeared to exhibit different emission behavior (orange and dull yellow). The luminescence behavior, including lifetimes, of **1**, **2**, **3a**, and **3b** was studied at ambient and liquid nitrogen temperatures. The results are summarized in Table 5 and in Figures 10 and 11. Figure 10 shows excitation and emission traces for samples **1**, **2**, **3a**, and **3b** at 293 K and 77 K, highlighting thermochromism as well as compound specific behavior. For samples **3a** and **3b** at 77 K, dashed excitation traces correspond with dashed emission traces and solid excitation traces are likewise matched to solid emission traces. Figure 11 gives a closer view of compound specific emission of samples **1**, **2**, **3a**, and **3b** at 77 K.

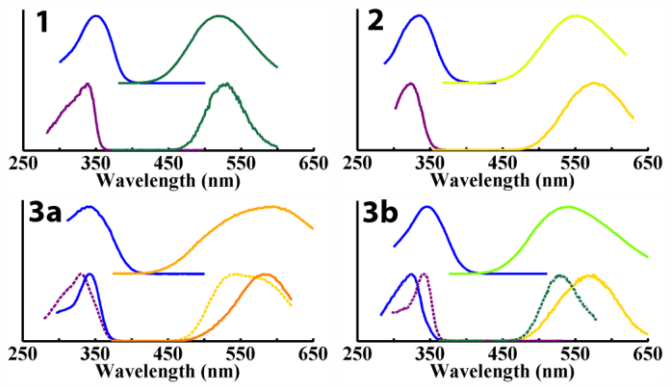

Fig. 10. Luminescence spectra showing normalized intensity (arbitrary units) for **1**, **2**, **3a**, and **3b** at 293 K (upper traces) and 77 K (lower traces).

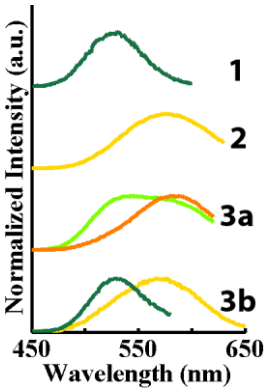

Fig. 11. Emission spectra of **1**, **2**, **3a**, and **3b** at 77 K.

Given their spectroscopic similarity to well-known ^{3}CC transitions seen for amine- and phosphine-substituted CuI clusters,[1,11b,12,13] the results here are interpreted likewise. Nevertheless, unlike nitrogen and phosphorus, sulfur donors bear an unused electron pair. Therefore, the possibility of ligand to Cu cluster transitions cannot strictly be ruled out without further computational study.

All four species showed moderate energy peak excitation wavelengths (335−350 nm). However, in all cases emission was seen at relatively low energies (LE band, 519−590 nm) depending on the compound. Bands that could be described as HE are uniformly absent; this is due to the fact that THT lacks π* ligand orbitals needed for XLCT or MLCT.[12,13]

Modest but fully reversible thermochromic effects were encountered for all compounds. At ambient temperature, compound **1** shows single excitation and emission bands at 350 nm and 519 nm, respectively, shifting to 339 nm and 528 nm at 77 K. Similarly, **2** revealed excitation and emission bands at 335 nm and 552 nm, shifting to 330 nm and 575 nm at 77 K. Compound **3a** displayed a very broad ambient temperature emission at 590 nm with peak excitation at 344 nm. This asymmetric emission band was found to split as the temperature was lowered to 77 K. The result was two coupled excitation/emission band pairs: 345/583 nm and 329/545 nm. Compound **3b** also showed splitting at reduced temperature. The ambient temperature excitation and emission bands at 346 nm and 541 nm split into two coupled excitation/emission band pairs: 341/529 nm and 324/576 nm. The emission band

splitting seen in **3a** and **3b** may be the result of symmetry lowering at reduced temperature. It is relevant to recall that compound **3a** is actually the lower symmetry **3a'** at this temperature.

To a first approximation the bands seen in these compounds are relatively similar to one another. Nevertheless, the subtle differences amongst them are instructive. Based on extensive precedent, the LE transitions seen may be attributed to ^{3}CC behavior. Previous studies have definitively shown that the ^{3}CC transition is itself a combination of XMCT and MC components.[12,13] Three metrics may be used to evaluate the contributions of these components: (1) Stokes shift, (2) thermochromic emission shift, and (3) emission lifetime. Because the XMCT involves transition from a largely I_n-cluster based HOMO to a largely Cu_n-cluster based LUMO (n = 2, 4, 6), it is accompanied by distortion of the cluster, resulting in a large Stokes shift. In addition, excited state cluster distortion brings the metal atoms into closer proximity to one another, increasing their degree of bonding and thus stabilizing the excited state. Longer wavelength emission is the result. A ^{3}CC transition that is more heavily MC ($3d^{10} \rightarrow 3d^9 4p^1$) would be expected to show a lesser degree of Stokes shift. ^{3}CC transitions usually have lifetimes near 10−20 μs. However, it seems likely that lifetimes are apt to be longer for the more disruptive XMCT than for the MC.

Phases **3a** and **3b** both show pairs of excitation/emission bands at reduced temperature. Considering **3b** at 77 K first, its pair of coupled bands shows differences in both Stokes shift and lifetime. The higher energy Stokes shift and longer lifetime (15.5 vs. 8.99 μs) belong to the lower energy (LE_1) 324/576 nm band (yellow emission). It is reasonable to assert that this ^{3}CC band has greater ^{3}XMCT character than does the higher energy band (LE_2) 341/529 nm band (green emission). Furthermore, it is reasonable that the longer lifetime be associated the more disruptive ^{3}XMCT process.

For phase **3a** at 77 K, it should be noted we are actually considering phase **3a'** given the conversion noted in the crystallographic observations discussed above. Unlike **3b** in which LE_2 emission is associated with the higher energy excitation band, in **3a'** LE_2 is associated with the *lower* energy

excitation band. The two bands for **3a'** show similar Stokes shifts (LE_1 = 12,100 and LE_2 = 12,000 cm^{-1}), but different lifetimes (LE_1 = 15.0 μs and LE_2 = 9.97 μs). Thus, using the criteria established above, there appears to be a more even balance between ^{3}XMCT and ^{3}MC character in the CC bands for **3a**.

At 77 K, compound **2** also shows a relatively large Stokes shift (12,900 cm^{-1}) and long lifetime (15.5 μs), and therefore should be regarded as largely ^{3}XMCT in character. At 77 K the cubane network complex **1** shows a more modest Stokes shift (10,600 cm^{-1}) and a shorter lifetime (10.4 μs). These values are similar to those of the LE_2 band for **3b** and thus should be seen as being more ^{3}MC in nature.

Conclusions

The CuI-THT system (from MeCN) is comprised of at least six distinct phases: green-emitting $(CuI)_4(THT)_2$ (**1**), yellow-emitting $(CuI)_{10}(THT)_7(MeCN)$ (**2**), orange-emitting $(CuI)_4(THT)_4$ (**3a**), dull yellow-emitting $(CuI)_4(THT)_4$ (**3b**), non-emissive $(CuI)_3(THT)_3$•MeCN (**4**), and non-emissive $(CuI)_2(THT)_4$ (**5**). Compound **1** is a 3-D network consisting of Cu_4I_4 cubane units and μ_2-THT ligands. Compound **2** is a 1-D ladder consisting of $\{[Cu_4I_4(THT)](\mu_2\text{-}THT)_2(Cu_2I_2)(\mu_2\text{-}THT)_2[Cu_4I_4(NCMe)]\}$ rungs connected by pairs of μ_2-THT links. Compounds **3a** and **3b** are simple $(CuI)_4(THT)_4$ molecules. Denser triclinic **3b** is more stable than monoclinic **3a** phase at 25 °C, converting to **3a** at ≥38 °C. **3a** shows a transformation to a triclinic phase (**3a'**) that retains orange emission at −60 °C. Compound **4** is a 2-D sheet containing $Cu_3(THT)_3$ rings trigonally linked by rhomboid Cu_2I_2 dimer units with MeCN solvent molecules occupying large $(Cu_2I_2)_6(THT)_6$ rings. The dimer **5** consists of a Cu_2I_2 rhomboid core decorated with four THT ligands. Precipitation of CuI/THT mixtures from MeCN shows a trend with increasing temperature: **4** → **3b** → **3a** → **2** → **1**. CuI-rich conditions, either during precipitation or solid state grinding favor the formation of **1**. In contrast, reaction of CuI with neat THT or grinding of any of

the other solid phases in excess THT produces **5**.

Compounds **1**, **2**, **3a**, and **3b** are all photoemissive, showing long wavelength emission (519−590 nm) stimulated by near UV excitation (335−350 nm) at room temperature. These bands are attributed to cluster centered transitions which combine halide-to-ligand (XMCT) and metal-centered (MC) components. Both **3a** and **3b** show splitting into coupled pairs of excitation/emission bands at 77 K. It is hypothesized that the larger Stokes shift-longer lifetime features are associated with greater XMCT character.

ACKNOWLEDGMENT Grateful acknowledgement is made to National Science Foundation (CHE-0848109, RDP), (CHE-0351877, HHP), and the Virginia Space Grant Consortium (student awards to CW and KMH). Research at GWU is supported by the Office of Basic Energy Sciences of the U.S. Department of Energy as part of the Materials Science of Actinides Energy Frontier Research Center (DE-SC0001089). We are indebted to NSF (CHE-0443345) and the College of William and Mary for the purchase of the X-ray equipment. Special thanks are extended to Dr. Fred Hollander (Univ. of California, Berkeley) for his help with modeling of crystallographic disorder.

SUPPORTING INFORMATION AVAILABLE Additional crystallographic views of compounds **1**, **2**, **3a**, **3b**, and **4**, experimental-calculated PXRD comparisons for compounds **1**, **2**, **3a**, **3b**, **4**, and **5**.

References

1. Safko, J. P.; Kuperstock, J. E.; McCullough, S. M.; Noviello, A. M.; Li, X.; Killarney, J. P.; Murphy, C.; Patterson, H. H.; Bayse, C. A.; Pike, R. D. *Dalton Trans.* **2012**, *41*, 11663−11674.
2. (a) Araki, H.; Tsuge, K.; Sasaki, Y.; Ishizaka, S.; Kitamura, M. *Inorg. Chem.* **2005**, *44*, 9667−9675. (b) Hu, S.; Tong, M.-L. *Dalton Trans.* **2005**, 1165−1167. (c) Araki, H.; Tsuge, K.; Sasaki, Y.; Ishizaka, S.; Kitamura, M. *Inorg. Chem.* **2007**, *46*, 10032−10034. (d) Peng, R.; Li, M.; Li, D. *Coord. Chem. Rev.*

2010, *254*, 1−18. (e) Perruchas, S.; Tard, C.; Le Goff, X. F.; Fargues, A.; Garcia, A.; Kahlal, S.; Saillard, J.-Y.; Gacoin, T.; Boilot, J.-P. *Inorg. Chem.* **2011**, *50*, 10682−10692. (f) Liu, Z.; Djurovich, P. I.; Whited, M. T.; Thompson, M. E. *Inorg. Chem.* **2012**, *51*, 230−236. (g) Tsuge, K. *Chem. Lett.* **2013**, *42*, 204−208.

3. Killarney, J. P.; McKinnon, M.; Murphy, C.; Henline, K. M.; Wang, C.; Pike, R. D.; Patterson, H. H. *Inorg. Chem. Commun.* **2014**, *40*, 18−21.
4. Norén, B.; Oskarsson, Å. *Acta. Chem. Scand. Ser. A* **1987**, *41*, 12–17.
5. Paulsson, H.; Berggrund, M.; Fischer, A.; Kloo, L. *Z. Anorg. Allg. Chem.* **2004**, *630*, 413–416.
6. (a) Suenaga, Y.; Maekawa, M.; Kuroda-Sowa, T.; Munakata, M.; Morimoto, H.; Hiyama, N.; Kitagawa, S. *Anal. Sci.* **1997**, *13*, 651−652. (b) Heller, M.; Sheldrick, W. S. *Z. Anorg. Allg. Chem.* **2004**, *630*, 1869−1874. (c) Lu, W.; Yan, Z.-M.; Dai, J.; Zhang, Y.; Zhu, Q.-Y.; Jia, D.-X.; Guo, W.-J. *Eur. J. Inorg. Chem.* **2005**, 2339–2345. (d) Lee, S. Y.; Park, S.; Lee, S. S. *Inorg. Chem.* **2009**, *48*, 11335−11341. (e) Jo, M.; Seo, J.; Lindoy, L. F.; Lee, S. S. *Dalton Trans.* **2009**, 6096−6098. (f) Martínez-Alanis, P. R.; Ugalde-Saldívar, V. M.; Castillo, I. *Eur. J. Inorg. Chem.* **2011**, 212−220.
7. Boorman, P. M.; Kerr, K. A.; Kydd, R. A.; Moynihan, K. J.; Valentine, K. A. *J. Chem. Soc., Dalton Trans.* **1982**, 1401−1405.
8. See for example (a) Kim, T. H.; Shin, Y. W.; Lee, S. S.; Kim, J. *Inorg. Chem. Commun.* **2007**, *10*, 11−14. (b) Kim, T. H.; Shin, Y. W.; Jung, J. H.; Kim, J. S.; Kim, J. *Angew. Chem. Int. Ed.* **2008**, *47*, 685−688. (c) Xie, C.; Zhou, L.; Feng, W.; Wang, J.; Chen, W. *J. Mol. Struct.* **2009**, *921*, 132−136. (d) Zhang, J.; Xue, Y.-S.; Li, Y.-Z.; Du, H.-B.; You, X.-Z. *CrystEngComm* **2011**, *13*, 2578−2585.
9. (a) Knorr, M.; Guyon, F.; Khatyr, A.; Däschlein, C.; Strohmann, C.; Aly, S. M.; Abd-El-Aziz, A. S.; Fortin, D.; Harvey, P. D. *Dalton Trans.* **2009**, *38*, 948−955. (b) Knorr, M.; Guyon, F.; Kubicki, M. M.; Rousselin, Y.; Alyc, S. M.; Harvey. P. D. *New J. Chem.* **2011**, *35*, 1184−1188. (c) Aly, S. M.; Pam, A.; Khatyr, A.; Knorr, M.; Rousselin, Y.; Kubicki, M. M.; Bauer, J. O.; Strohmann, C. D.; Harvey, P. D. *J. Inorg. Organomet. Polym. Mater.* **2014**, in press (DOI: 10.1007/s10904-013-9984-9).

10. (a) Maelger, H.; Olbrich, F.; Kopf, J.; Abeln, D.; Weiss, E. *Z. Naturforsch. B* **1992**, *47*, 1276−1280. (b) Zhou, J.; Bian, G.-Q.; Dai, J.; Zhang,Y.; Zhu, Q.-Y.; Lu, W. *Inorg. Chem.* **2006**, *45*, 8486−8488.
11. (a) Filippo, J. S., Jr.; Zyontz, L. E.; Potenza, J. *Inorg. Chem.* **1975**, *14*, 1667−1671. (b) Knorr, M.; Pam, A.; Khatyr, A.; Strohmann, C.; Kubicki, M. M.; Rousselin, Y.; Aly, S. M.; Fortin, D.; Harvey, P. D. *Inorg. Chem.* **2010**, *49*, 5834−5844.
12. (a) Ford, P. C.; Cariati, E.; Bourassa, J. *Chem. Rev.* **1999**, *99*, 3625−3647. (b) Vitale, M.; Ford, P. C. *Coord. Chem. Rev.* **2001**, *219−221*, 3−16. (c) Angelis, F. D.; Fantacci, S.; Sgamellotti, A.; Cariati, E.; Ugo, R.; Ford, P. C. *Inorg. Chem.* **2006**, *45*, 10576−10584.
13. (a) Vega, A.; Saillard, J.-Y. *Inorg. Chem.* **2004**, *43*, 4012−4018. (b) Perruchas, S.; Tard, C.; Le Goff, X. F.; Fargues, A.; Garcia, A.; Kahlal, S.; Saillard, J.-Y.; Gacoin, T.; Boilot, J.-P. *Inorg. Chem.* **2011**, *50*, 10682−10692. (c) Liu, Z.; Djurovich, P. I.; Whited, M. T.; Thompson, M. E. *Inorg. Chem.* **2012**, *51*, 230−236.
14. *SMART Apex II, Data Collection Software*, version 2.1; Bruker AXS Inc.: Madison, WI, 2005.
15. *SAINT Plus, Data Reduction Software*, version 7.34a; Bruker AXS Inc.: Madison, WI, 2005.
16. Sheldrick, G. M. *SADABS*; University of Göttingen: Göttingen, Germany, 2005.
17. Altomare, A.; Cascarano, G.; Giacovazzo, C.; Gualardi, A. *J. Appl. Cryst.* **1993**, *26*, 343−350.
18. Sheldrick, G. M. *Acta Crystallogr., Sect. A* **2008**, *64*, 112–122.
19. Hübschle, C. B.; Sheldrick, G. M.; Dittrich, B. *J. Appl. Cryst.* **2011**, *44*, 1281−1284.
20. *JADE*, version 6.1 Materials Data Inc. Livermore, CA, 2002.
21. *DIFFRAC Plus*, version 10.0 and *EVA*, release 2004; Bruker AXS Inc.: Madison, WI, 2005.
22. Macrae, C. F.; Bruno, I. J.; Chisholm, J. A.; Edgington, P. R.; McCabe, P.; Pidcock, E.; Rodriguez-Monge, L.; Taylor, R.; van de Streek, J.; Wood, P. A. *J. Appl. Cryst.* **2008**, *41*, 466−470.
23. Spek, A. L. *J. Appl. Cryst.* **2003**, *36*, 7−13.
24. Maini, L.; Braga, D.; Mazzeo, P. P.; Ventura, B. *Dalton Trans.* **2012**, *41*, 531−539.
25. Nelyubina, Y. V.; Glukhov, I. V.; Antipin, M. Yu.; Lyssenko, K. A. *Chem. Commun.* **2010**, *46*,

3469−3471.

Table 1. Crystal and structure refinement data[a]

	1	**2**	**3a**
CCDC deposit no.	977480	977481	977482
color and habit	colorless block	colorless prism	colorless prism
size, mm	0.35 × 0.25 × 0.23	0.38 × 0.12 × 0.09	0.35 × 0.16 × 0.15
Formula	$C_8H_{16}Cu_4I_4S_2$	$C_{30}H_{59}Cu_{10}I_{10}NS_7$	$C_{16}H_{32}Cu_4I_4S_4$
formula weight	938.09	2562.60	1114.41
space group	$P2_12_12_1$(#19)	$P2_1/m$ (#11)	$P2_1/n$ (#14)
a, Å	11.7527(2)	11.9107(4)	9.5824(2)
b, Å	11.8972(2)	12.2273(4)	34.9161(6)
c, Å	13.3762(2)	21.0371(6)	17.9841(3)
α, deg	90	90	90
β, deg	90	97.434(2)	91.2810(10)
γ, deg	90	90	90
volume, Å^3	1870.32(5)	3038.00(17)	6015.62(19)
Z	4	2	8
ρ_{calc}, g cm^{-3}	3.331	2.801	2.461
F_{000}	1696	464	4160
μ(Cu Kα), mm^{-1}	58.888	46.043	38.037
temperature, K	100	123	250
residuals:[a] R; R_w	0.0458; 0.1169	0.0545; 0.1531	0.0476; 0.1182
goodness of fit	1.080	1.140	1.064

Flack parameter	0.862(12)	–	–

[a]R = $R_1 = \Sigma||F_o| - |F_c||/ \Sigma|F_o|$ for observed data only. $R_w = wR_2 = \{\Sigma[w(F_o^2 - F_c^2)^2]/\Sigma[w(F_o^2)^2]\}^{1/2}$ for all data.

Table 1. Cont'd

	3b	**4**
CCDC deposit no.	977483	977484
color and habit	colorless prism	colorless block
size, mm	0.31× 0.12× 0.09	0.47 × 0.29 × 0.19
Formula	$C_{16}H_{32}Cu_4N_4S_4$	$C_{14}H_{27}Cu_3I_3NS_3$
formula weight	1114.42	876.86
space group	*P*−1(#2)	*C*2/*c* (#15)
a, Å	9.5915(2)	22.7901(7)
b, Å	10.8378(3)	13.2617(4)
c, Å	15.7597(4)	16.0147(5)
α, deg	73.2170(10)	90
β, deg	72.4319(12)	90.1331(11)
γ, deg	69.2273(11)	90
volume, $Å^3$	1429.64(6)	4840.2(3)
Z	2	8
ρ_{calc}, g cm^{-3}	2.589	2.407
F_{000}	1040	3296
μ(Cu Kα), mm^{-1}	40.013	35.514
temperature, K	100	100
residuals:[a] R; R_w	0.0501; 0.1621	0.0304; 0.0785
goodness of fit	1.163	1.175

Flack parameter	–	–

[a]R = $R_1 = \Sigma||F_o| - |F_c||/ \Sigma|F_o|$ for observed data only. $R_w = wR_2 = \{\Sigma[w(F_o^2 - F_c^2)^2]/\Sigma[w(F_o^2)^2]\}^{1/2}$ for all data.

Table 2. Selected bond lengths (Å) and angles (°) for all complexes.

	1	**2**[a]	**3a**	**3b**	**4**	**5**[b]
Cu−I	2.610(2)-2.756(3)	2.6098(14)-2.703(15)	2.6469(16)-2.709(3)	2.650(3)-2.728(3)	2.5887(8)-2.6418(7)	2.637(1), 2.639(1)
Cu−S	2.312(4), 2.317(4), 2.325(4)	2.307(4)-2.361(6)	2.284(3)-2.380(7)	2.292(4), 2.293(4), 2.302(4), 2.306(4)	2.3187(11)-2.3517(10)	2.318(2), 2.331(3)
Cu···Cu	2.636(3)-2.759(3)	2.650(5)-2.754(3)	2.6728(19)-2.837(3)	2.639(3)-2.768(3)	2.9653(14), 2.9722(9)	2.675(2)
I−Cu−I	107.31(8)-118.02(9)	110.77(7)-120.76(11)	108.06(8)-116.29(6)	109.67(9)-118.22(9)	110.40(2), 110.79(3), 110.86(2)	119.08(4)
Cu−I−Cu	58.07(7)-62.20(7)	58.61(7)-63.67(6), 92.70(8), 97.58(7)	59.55(4)-64.09(5)	58.29(7)-62.30(7)	69.06(3), 69.27(2), 69.43(2)	60.92(4)
I−Cu−S	93.64(12)-117.00(13)	98.04(9)-124.26(17)	87.44(17)-118.81(16)	98.97(13)-114.32(13)	107.04(4)-113.51(4)	104.6(1), 104.7(1), 104.7(1), 109.6(1)
S−Cu−S	−	98.96(17), 99.08(15), 105.39(19)	−	−	102.49(4), 104.10(4), 104.64(5)	114.5(1)
Cu−S−Cu	120.47(17), 124.08(18)	117.51(18)-123.27(13)	−	−	120.26(5), 121.40(5), 128.78(5)	−

[a]Bonding to Cu9 (10% occupancy) omitted. [b]Data from ref. 4.

Table 3. Unit cell parameters for $(CuI)_4(THT)_4$ cubane polymorphic phases.

	3a	**3a'**[a]	**3b**
Temp., K	250	200	100
Space group	$P2_1/n$	triclinic P	$P-1$
a, Å	9.5824(2)	9.69	9.5852(5)
b, Å	34.9161(6)	16.38	10.8359(5)
c, Å	17.9841(3)	36.39	15.7749(8)
α, °	90	87.48	73.253(2)
β, °	91.2810(10)	88.27	72.470(2)
γ, °	90	88.66	69.213(2)
Volume, $Å^3$	6015.62(19)	5858	1430.15(12)
Z	8	(8)	2

[a]Limited data set, structure solution not pursued.

Table 4. Grinding and vacuum study results.

Initial Compound	Dry Grinding Product	Grinding Product with Drop of THT	Grinding Product with Excess THT	Vacuum Treatment (50 mTorr)
1	**1**	**3a**	**5**	**1**
2	**1**	**3a**	**5**	**2**
3a	**3a/3b**	**3a**	**5**	**1**
3b	**1**	**3a**	**5**	**1**

Compound	T (K)	λ_{em} (nm), [λ_{ex} (nm)]	Stokes Shift (cm^{-1})	Lifetime (μs)
$(CuI)_4(THT)_2$, **1**	293	519, [350]	9,700	12.1
	77	528, [339]	10,600	10.4
$(CuI)_{10}(THT)_7(MeCN)$, **2**	293	552, [335]	11,700	23.7
	77	575, [330]	12,900	15.5
$(CuI)_4(THT)_4$, **3a**	293	590, [344]	10,200	19.1
	77	583, [345]	12,100	15.0
	77	545, [329]	12,000	9.97
$(CuI)_4(THT)_4$, **3b**	293	541, [346]	10,400	6.60
	77	529, [341]	10,400	8.99
	77	576, [324]	13,500	15.5

For Table of Contents Use Only

Structure, Dynamics, and Photophysics in the Copper(I) Iodide-Tetrahydrothiophene System.

Kylie M. Henline, Charles Wang, Robert D. Pike,* John C. Ahern, Bryer Sousa, Howard H. Patterson, Andrew T. Kerr, and Christopher L. Cahill

SYNOPSIS TOC: Multiple crystalline phases, including bridged networks and polymorphic Cu_4I_4 tetramers, result from the reaction of CuI and tetrahydrothiophene (THT). Formation of the various phases from solution as a function of temperature and mixing ratio is studied, as is luminescence emission behavior.